

## Article

# Advancing Sustainable Marine Exploration: Highly Efficient Photonic Radar for Underwater Navigation Systems under the Impact of Different Salinity Levels

Aras Aldawoodi <sup>1,2,\*</sup> and Hasan Şakir Bilge <sup>3</sup><sup>1</sup> Computer Science, Graduate School of Informatics, Gazi University, Ankara 06570, Turkey<sup>2</sup> Department of Computer Science, College of Computer Science and Information Technology, University of Kirkuk, Kirkuk 36001, Iraq<sup>3</sup> Engineering Faculty, Electrical-Electronics Engineering, Gazi University, Ankara 06570, Turkey; bilge@gazi.edu.tr

\* Correspondence: aghazi.aldawoodi@gazi.edu.tr

**Abstract:** The exploration of underwater environments for applications like environmental monitoring, scientific research, and surveillance has propelled the significance of underwater wireless navigation. Light waves have emerged as a promising solution, offering the potential to achieve the required data rates and propagation speeds. However, underwater optical wireless navigation faces challenges, particularly limited range. This research investigates a novel FMCW (frequency-modulated continuous wave)-based photonic radar system's efficacy in detecting underwater vehicles across diverse salinity levels and distances. Numerical simulation evaluations reveal distinct signal-to-noise ratios (SNR) and detected power peaks corresponding to varying salinity levels, demonstrating the system's sensitivity. At 5 g/L salinity, the detected power peaked at  $-95$  dBm, decreasing to  $-105$  dBm at 15 g/L. SNR analysis indicates robust detection within a 4 m range, with challenges emerging at extended ranges and higher salinity. Despite these challenges, the system shows promise for near-range underwater navigation, contributing to sustainable marine exploration by enhancing the accuracy and efficiency of underwater monitoring systems. This advancement aligns with the goals of sustainable development by supporting the protection of marine ecosystems, promoting scientific understanding of underwater environments, and aiding in the sustainable management of marine resources.

**Keywords:** frequency-modulated continuous wave (FMCW); photonic radar; underwater communication; salinity; sustainable development



**Citation:** Aldawoodi, A.; Bilge, H.Ş. Advancing Sustainable Marine Exploration: Highly Efficient Photonic Radar for Underwater Navigation Systems under the Impact of Different Salinity Levels. *Sustainability* **2024**, *16*, 2851. <https://doi.org/10.3390/su16072851>

Academic Editors: Sushank Chaudhary, Muhammad Saadi and Vincenzo Barrile

Received: 23 January 2024

Revised: 16 March 2024

Accepted: 20 March 2024

Published: 29 March 2024



**Copyright:** © 2024 by the authors. Licensee MDPI, Basel, Switzerland. This article is an open access article distributed under the terms and conditions of the Creative Commons Attribution (CC BY) license (<https://creativecommons.org/licenses/by/4.0/>).

## 1. Introduction

The vastness of the world's oceans and the increasing demand for underwater activities highlight the integral role of navigation beneath the waves [1,2]. Submarines, autonomous underwater vehicles (AUVs), and remotely operated vehicles (ROVs) are vital for marine exploration, scientific research, and defense operations [3–5]. The growth of underseas infrastructure further emphasizes the need for accurate underwater navigation systems [6–8]. Efficient underwater navigation becomes a strategic imperative as nations explore and exploit resources in deeper waters [9,10]. In environmental monitoring, underwater vehicles are essential for studying marine ecosystems, tracking climate change effects, and ensuring the sustainability of underwater resources [1,11,12]. Advancements in underwater navigation technologies are vital for the successful management of these diverse underwater activities. Navigation underwater presents challenges due to the unique characteristics of water as a medium, including limited visibility and the impracticality of GPS [2,13,14]. Traditional acoustic navigation systems face signal degradation, interference,

and detection risks in defense applications [15,16]. Intricate underwater topography, including caves and trenches, requires technology capable of providing accurate, real-time solutions. Underwater acoustic communication has traditionally dominated, but suffers from high latency and low data rates [17–19]. Underwater radio frequency (RF) communication faces severe attenuation, leading to a limited transmission distance [20–23]. In contrast, underwater optical wireless communication (UOWC) presents itself as a natural candidate, offering higher data rates and shorter latency. UOWC is cost-effective and power-effective, utilizing low-cost, low-power transceivers like LEDs and photodiodes [24]. Despite these advantages, the limited transmittance of optical waves and challenges posed by shorter wavelengths demand focused research on improving UOWC system performance [25,26]. UOWC technology, with its potential for high bandwidth and data rates, is attractive for marine applications including underwater wireless sensor networks, oil and gas industry monitoring, underwater drones, and pollution monitoring [15,27]. However, the turbulent nature of the underwater channel poses challenges, impacting signal performance and increasing the bit error ratio (BER).

Photonic radar is emerging as a cutting-edge solution for underwater navigation, leveraging radar principles with light instead of radio waves [28]. This technology overcomes the limitations of traditional acoustic systems, offering higher resolution and accuracy, even in turbid waters. Photonic radar operates in low-light conditions, penetrating water more effectively than traditional imaging technologies, which is crucial for avoiding obstacles and navigating challenging terrains. Photonic radar systems, less susceptible to interference compared to acoustics, are advantageous in defense applications where stealth and reliability are paramount [29–31]. As human activities expand into the depths of oceans, addressing underwater navigation challenges becomes imperative. Photonic radar's capacity to provide accurate, real-time navigation information positions it as a promising solution. Some key works on photonic radar in autonomous systems are listed as follows.

The technology explored in 2021 by the authors of [32], photonic radar, is gaining traction as a next-gen radar, surpassing conventional limitations. This study presents the design and implementation of an X-band photonic radar for real-time, high-resolution imaging and low radar cross-section (RCS) target detection. Utilizing photonic frequency quadrupling and advanced signal processing, the radar successfully detected a low-RCS drone at a distance of 2.7 km in field experiments, demonstrating its potential for enhanced surveillance. In another ground-breaking study [33], researchers proposed a cost-effective Photonic Radar for future transportation, integrating Frequency Modulated Continuous Wave technology. Utilizing Wavelength and Polarization Division Multiplexing, the system demonstrated the efficient detection of multiple targets through numerical simulations. Its effectiveness in detection, ranging, and resolution was validated over 100 m with varying bandwidths. Another study [34] delves into the principles of frequency-modulated continuous wave photonic radar, emphasizing its benefits. Mathematical analysis and numerical simulations of the direct detection and coherent detection schemes reveal trade-offs, in which direct detection offers simplicity but compromises sensitivity, while coherent detection excels in target range and velocity estimation at the expense of increased complexity. Authors in [35] proposed a coherent detection-based linear frequency modulated continuous wave (LFMCW) photonic radar for autonomous vehicles, emphasizing obstacle detection in challenging conditions. Utilizing polarization division multiplexing (PDM), the system successfully detects multiple targets in zero visibility with atmospheric turbulence. Results showcase effective detection under varying traffic speeds, with a reported range resolution of 15 cm at 1 GHz and 6.75 cm at 4 GHz over a distance of 100 m. The author in [36] addresses the surge in global road accidents by proposing high-speed photonic radar with a cost-effective wavelength division multiplexing (WDM) scheme for multiple target detection under adverse weather conditions. Numerical simulations showcase the radar's performance in received power, signal-to-noise ratio (SNR), and at a range resolution of 7 cm at an 80 m distance. Comparative analysis with traditional microwave

radar validates the proposed photonic radar's effectiveness. Addressing the challenge of real-time detection and tracking of multiple targets in urban environments for autonomous vehicles (AVs), this study [37] presents a photonic radar system using direct detection and frequency-modulated continuous wave (FMCW) with three transmission channels. Employing wavelength division multiplexing (WDM) for multiplexing, the system demonstrates the successful detection of multiple stationary targets in adverse weather conditions, with electronic equalization mitigating atmospheric attenuation, resulting in a 54% increase in received power. Another study [38] explores the demand for photonic radar systems in radar applications, emphasizing real-time high-resolution target detection. The frequency-modulated continuous-wave photonic radar system with coherent detection is theoretically investigated, considering atmospheric weather attenuations and solar background noise. Simulations under various atmospheric conditions reveal practical limitations, highlighting the potential of photonic radar for applications such as autonomous vehicle radar systems and navigation.

This paper explores the application of photonic radar properties in underwater navigation. As far as the authors are aware, photonic radar has not been employed in underwater navigation to date. Photonic radar systems in underwater environments face challenges due to varying salinity levels. Salinity affects signal attenuation, leading to reduced range and sensitivity. Changes in the refractive index due to salinity variations can cause signal distortion and scattering, impacting detection accuracy. Accurate system calibration is essential to compensate for these effects. Environmental factors such as temperature and turbidity, along with biological organisms, can further interfere with system performance. High salinity levels limit the penetration depth of optical signals, restricting the operational range. Overcoming these challenges requires advancements in photonics, signal processing, and underwater sensing technologies. The system was tested under different salinity levels in the underwater environment, and the study investigates the efficacy of the proposed photonic radar-based navigation. By delving into technological advancements, the paper aims to elucidate photonic radar's potential to revolutionize underwater navigation across areas including marine exploration, defense operations, and environmental monitoring.

## 2. System Description

Figure 1 shows the schematic diagram of the proposed photonic radar, which represents a cutting-edge fusion of optical and radio frequency (RF) technologies, tailored specifically for the detection of underwater vehicles. This advanced system leverages precision and the speed of light to provide unparalleled detection capabilities in a marine environment.

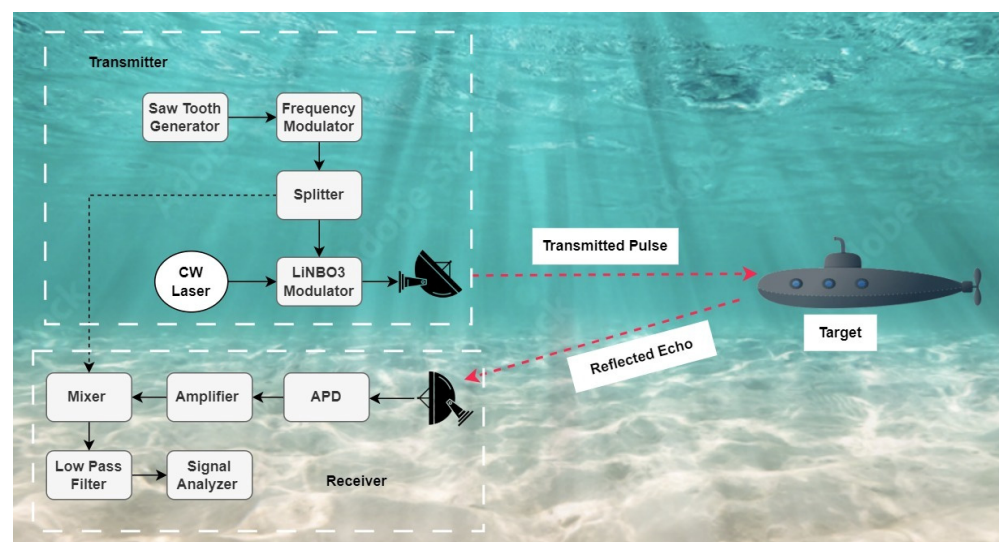


**Figure 1.** Proposed FMCW-based photonic radar for underwater optical navigation.

At its core, a pseudo random signal is modulated by a sawtooth generator and a frequency modulator to create the necessary signal waveform. The RF spectrum of this signal is shown in Figure 2.

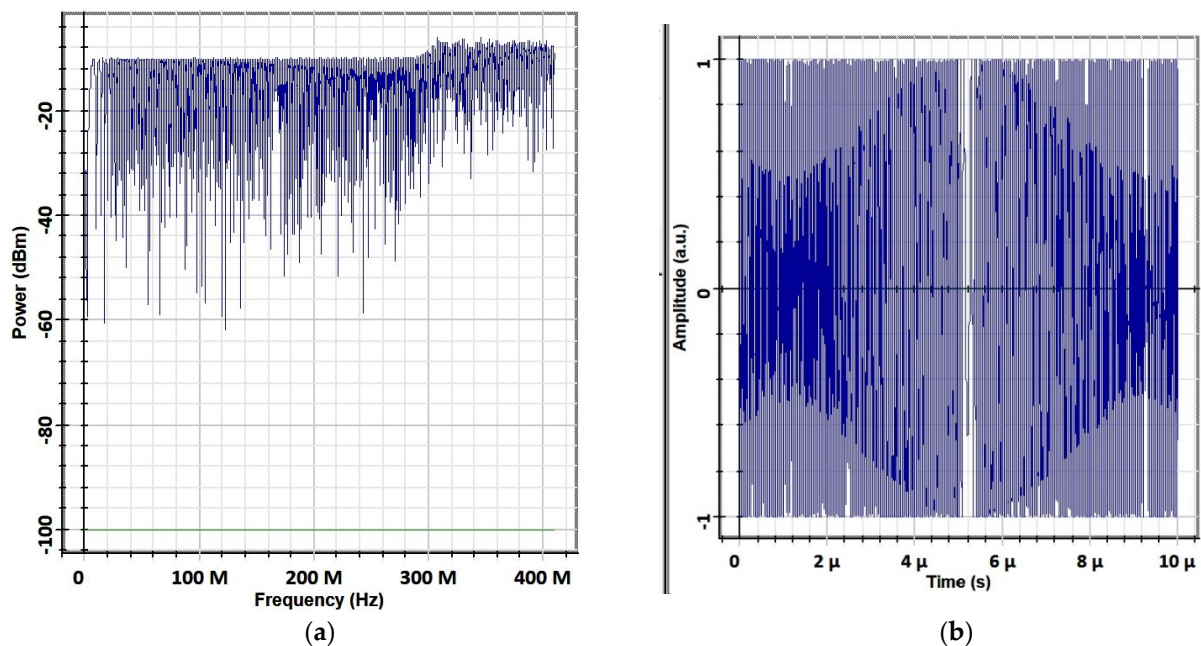


Figure 2. Transmitter: (a) RF spectrum and (b) radar signal on the oscilloscope.

At this stage, the RF signal is split into two parts. One part is directed towards the Mach-Zander modulator (MZM), while the other is used as a local oscillator for the mixing process in the receiver. The photonic radar utilizes a continuous-wave (CW) laser as its light source for carrying the RF signal. This laser signal from the CW source is routed through MZM. A lithium niobate ( $\text{LiNbO}_3$ ) modulator is used as the MZM, as it is a component known for its high electro-optic coefficient, which facilitates the effective modulation of the light. This output-modulated signal is focused towards the target using a telescope. The optical spectrum of the generated signal is shown in Figure 3.

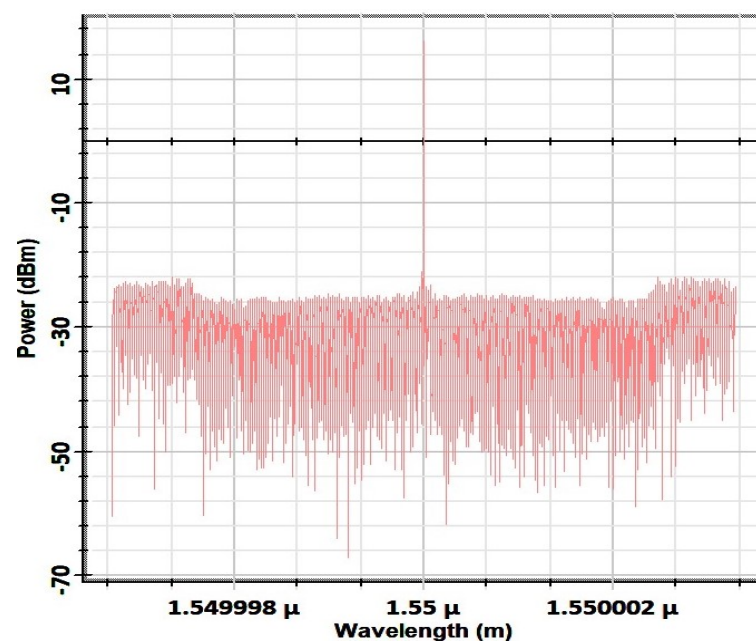


Figure 3. Optical spectrum.

The transmitted pulse travels through the aquatic environment, encountering various degrees of salinity which affect its propagation. The establishment of an underwater wireless optical connection can encounter substantial hurdles. A primary obstacle is the pronounced influence of the water's optical properties and the turbulence-related disturbances on the optical signal [39]. The propagation of optical signals in aquatic environments is greatly affected by two key factors: absorption and scattering. These factors are quantified by the absorption and scattering coefficients, symbolized as  $a(\lambda)$  and  $b(\lambda)$ , respectively, where  $\lambda$  represents the signal's wavelength. The cumulative impact of these coefficients on the optical signal is encapsulated by the beam extinction coefficient, symbolized as  $c(\lambda)$ . This coefficient,  $c(\lambda)$ , effectively measures the total attenuation that the optical signal undergoes in water, accounting for both absorption and scattering effects, as depicted in the equation below [40]:

$$c(\lambda) = a(\lambda) + b(\lambda), \quad (1)$$

The absorption coefficient, denoted as  $a(\lambda)$ , quantifies the extent to which light is absorbed in water, a process that varies with the properties of the water and the wavelength of the signal. On the other hand, the scattering coefficient, represented by  $b(\lambda)$ , reflects the degree of light scattering caused by waterborne particles, particularly when the size of these particles is on par with the wavelength of the light. The beam extinction coefficient, expressed as  $c(\lambda)$ , integrates the effects of both absorption and scattering coefficients, thereby offering a holistic view of the total attenuation that optical signals encounter in underwater environments. The overall absorption,  $a(\lambda)$ , in underwater optical communication systems is subject to a variety of influences, as detailed in the equation below [41]:

$$a(\lambda) = C_w a_w(\lambda) + C_{phy} a_{phy}(\lambda) + C_g a_g(\lambda) + C_n a_n(\lambda), \quad (2)$$

Here,  $a_w$  represents the absorption attributed to pure water itself,  $a_{phy}$  denotes the absorption caused by phytoplankton,  $a_g$  refers to absorption by dissolved organic matter, and  $a_n$  signifies absorption due to non-algal suspended particles. Each component plays a role in the total weakening of optical signals in marine environments. The coefficients  $C_w$ ,  $C_{phy}$ ,  $C_g$ , and  $C_n$ , respectively, stand for the absorption coefficients related to pure water, phytoplankton, dissolved organic matter, and non-algal suspended particles. The scattering of light in water is primarily dependent on the size of the particles present. For particles smaller than the optical wave's wavelength, the process is known as Rayleigh scattering. In contrast, Mie scattering occurs when particle sizes exceed the wavelength of the light used. Different oceanic regions have suspended particles of varying sizes. In the context of pure ocean water, which primarily contains salts and ions, these are generally comparable in size to the wavelength of the light used. Therefore, Rayleigh scattering is the most applicable description of scattering in such situations [42]. The formula for calculating the Rayleigh scattering coefficient in pure ocean water can be expressed as follows [40]:

$$b_w(\lambda) = 0.005826 \left( \frac{400}{\lambda} \right)^{4.322}, \quad (3)$$

The formula given determines the Rayleigh scattering coefficient, which is calculated based on the wavelength measured in nanometers. Although scattering greatly influences shorter wavelengths, absorption is predominantly responsible for the overall weakening of signals in pure ocean water. In coastal ocean waters, where there is a higher concentration of particulate and organic materials, scattering becomes the main cause of signal attenuation for optical waves. This scattering effect in ocean waters is considerably affected by the mix of organic and inorganic particles present. Furthermore, the optical properties of seawater are also influenced by factors like salinity, pressure, and temperature, which alter its refractive index. This change in refractive index creates an optical boundary that modifies the original trajectory of the optical wave. In these conditions, Mie scattering is the more accurate model to describe the scattering behavior. The coefficients for scattering, for both smaller and larger particles in seawater, are represented by distinct formulas, capturing the nuances of these different scattering mechanisms [40]:

$$b_l(\lambda) = 1.51302 \left( \frac{400}{\lambda} \right)^{1.17}, \quad (4)$$

$$b_s(\lambda) = 0.341074 \left( \frac{400}{\lambda} \right)^{0.3}, \quad (5)$$

In this context, the term  $b_l$  refers to the scattering coefficient for larger particles, while  $b_s$  indicates the scattering coefficient for smaller ones. Beyond absorption and scattering, the factor of turbulence is critical in affecting underwater optical wireless communication (UWOC). The underwater medium is subject to variations in temperature, density, and salinity, all of which lead to refractive index fluctuations in the underwater channel. These fluctuations, in turn, result in intensity variations of the received signal, a phenomenon known as turbulence [43,44]. Additionally, the presence of air bubbles in the water can cause random changes in the refractive index, further impacting UWOC performance. Understanding and analyzing the impact of turbulence is essential for improving UWOC systems. Salinity, defined by the amount of dissolved salts in water, is typically measured in parts per thousand (ppt) or as kilograms of salt per 1000 kg of water. Another unit used is the practical salinity unit (psu), nearly synonymous with ppt [45]. Ocean water salinity generally varies, ranging from 31 to 37 ppt. In polar regions, it often falls below 30 ppt, while in the Antarctic areas, it is around 34 ppt. Salinity can be determined through two primary methods. The first involves measuring the electrical conductivity (EC), given in micro-siemens per centimeter. The second assesses the total dissolved salts, quantifying the actual salt particles in the solution. Seawater's salt content typically includes chlorides, sulphates, and various carbonates like sodium, potassium, calcium, and magnesium. The average ocean water salinity is about 35 ppt [46], meaning that there are 35 g of dissolved substances in every 1000 g of seawater. In centimeter-gram-second (CGS) units, where water density is considered 1, this equates to roughly 35 g per liter (g/L).

Upon hitting the target, a portion of the light, determined by the target's reflectivity, is reflected back towards the source as an echo. This reflected echo is then captured by the receiver's aperture, which is carefully sized to optimize signal collection while minimizing noise. The returned signal, which exhibits a Doppler shift denoted as  $f_d = \frac{2v}{\lambda}$  and experiences a delay represented by  $\tau = \frac{2R}{c}$ , is captured by the telescope. This signal originates from a target in motion, positioned at a range distance  $R$  and moving at a velocity  $v$ . The intensity of this reflected signal, referred to as  $E_{ref}$ , is quantified as outlined in the equation below [47]:

$$E_{ref}(t) = \sqrt{P_r} \left[ 1 + \frac{\beta}{2} \cos(2\pi f_c (t - \tau) + \frac{\pi B}{T_m} (t - \tau)^2) \right] \cdot e^{j(\omega_o - \omega_d)t + \theta_o(t)}, \quad (6)$$

The receiver is equipped with an avalanche photodiode (APD), a highly sensitive component that converts the incoming optical signal into an electrical one, which is subsequently amplified for better detection. In a direct detection scheme, the receiver is relatively straightforward, functioning on the principle of square law detection without the need for optical mixing at the receiving end. The echoed signal is captured using a photodiode, which has a specific responsivity denoted by  $\mathfrak{R}$ . The resultant output photocurrent, symbolized as  $i_{ph}(t)$ , is described by the formula presented in the equation below [48]:

$$i_{ph}(t) = \mathfrak{R} \cdot P_r \left( 1 + \frac{\beta}{2} \cos(2\pi f_c (t - \tau) + \frac{\pi B}{T_m} (t - \tau)^2) \right)^2, \quad (7)$$

The baseband signal, derived from the filtered photocurrent signal, is defined as per the formulation in the equation below [49]:

$$i_{ph}(t) = I_{dc} + i_{sig}(t) \approx \mathfrak{R} \cdot P_r \left( 1 + \frac{\beta}{2} \cos(2\pi f_c (t - \tau) + \frac{\pi B}{T_m} (t - \tau)^2) \right)^2, \quad (8)$$

In this equation,  $i_{dc}$  represents the direct current (dc) component of the photocurrent, while  $i_{sig}$  refers to the alternating current (ac) component of the filtered signal.

The electrical signal is subsequently combined with the signal from the local oscillator. This process down-converts the signal's frequency to a more manageable level. Following this, the resulting beat signal, which passes through a low pass filter, is expressed in the equation below [47]:

$$S_b(t) = A_c \mathfrak{R} P_r \beta \cos(2\pi f_c \tau - \frac{\pi B}{T_m} \tau^2 + 2\pi f_r t), \quad (9)$$

In this equation,  $f_r$  represents the range frequency, which is computed using the formula provided in the equation below [50]:

$$f_r = \frac{2 \times R \times B}{T_m \times C}, \quad (10)$$

where  $B$  is system bandwidth. Figure 4 represents the signal after mixing at the receiver.

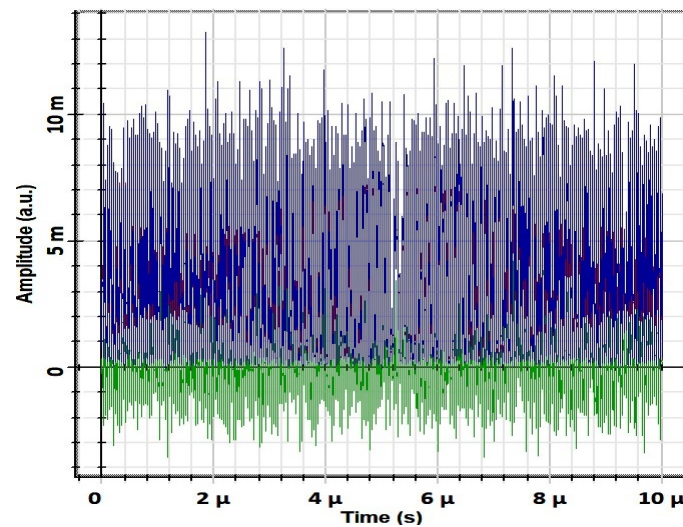


Figure 4. RF spectrum after mixing at the receiver.

Once filtered through a low-pass filter to eliminate high-frequency components that are not needed, the signal undergoes analysis to discern essential details about the target's presence and attributes. The performance of an FMCW-based photonic radar system utilizing a direct detection scheme is evaluated by calculating the signal-to-noise ratio (SNR) at the photodetector's output. Various types of noise are typically present in the detected signal, such as thermal noise, dark current noise, relative intensity noise (RIN), shot noise, and surface current noise [51]. In our SNR calculations, we focus on including both shot noise and thermal current noise, as detailed in the equation below [50]:

$$SNR_{dir} = \frac{\beta^2 \mathfrak{R}^2 P_r^2 / 2}{2q \mathfrak{R} P_r B_{rx} + 4k_b T_r B_{rx} / R_L}, \quad (11)$$

In this context,  $B_{rx}$  denotes the bandwidth of the receiver, and  $q$  represents the elementary electrical charge, approximately equal to  $1.6 \times 10^{-19}$  C (Coulombs). The Boltzmann constant,  $k_b$ , has a value of approximately  $1.38 \times 10^{-23}$  J/K (Joules per Kelvin).  $T_r$  refers to the noise temperature of the receiver, and  $R_L$  signifies the load resistance.

This system's performance was rigorously evaluated in MATLAB and OptiSystem under varying salinity levels, which simulated real-world marine conditions. The MATLAB-based Underwater Wireless Optical Communication (UWOC) model accounts for atmospheric loss, target reflectivity, optical transmission loss, and the physical parameters of the receiver. It incorporates a sophisticated algorithm to account for the attenuation caused by salt and alkaline concentration in the water. The algorithm adjusts the received signal power based on these parameters, ensuring that the system's sensitivity adapts to the envi-

ronment, providing reliable target detection even in challenging conditions. Parameters of different components considered in proposed photonic radar are given in Table 1.

**Table 1.** Underwater photonic radar modeling parameters.

Component	Parameter	Value
Continuous Wave Laser	Wavelength	1550 nm
	Linewidth	100 KHz
	Power	100 $\mu$ W
Dual Port Mech–Zhender Modulator (DP-MZM)	Extinction ratio	30 dB
	Switching bias voltage	4 v
	Switching RF voltage	4 v
	Bias voltage	0 v
Simulation Window	Sweep time	10 $\mu$ s
	No. of samples	8192
Photo detector (PIN)	Responsivity	1 A/W
	Dark current	1 nA
	Thermal and shot noise BW	410 MHz
	Absolute temp	290 k
	Load resistance	50 $\Omega$
Under Water Chanel Parameters	Atmospheric loss factor	0.5
	Target reflectivity	0.1
	Optical transmission loss	0.1
	Receiver aperture diameter	10 cm
	Salt concentration in clear water	0.5 g/L
	Alkaline concentration in clear water	8
Parameters		

### 3. Results and Discussion

In this section, we discuss the simulation results obtained from the proposed photonic radar-based underwater optical navigation system. To test the proposed system, we first considered clear ocean conditions with a salinity level chosen to be 0.2 g/L. The system is tested for an underwater range of 10 m and the system bandwidth is kept at 1 GHz. As shown in Figure 5, the graph presents the performance of the photonic radar system as a function of frequency, with the detected power in decibels-milliwatts (dBm) plotted along the Y-axis and the frequency along the X-axis, spanning a range from 5 to 9 MHz.

The radar system's response to an object in a medium with a salinity of 0.2 g/L is indicated by the red data points, whereas the green data points denote the noise floor of the system. A prominent peak is observed in the red curve at 6.67 MHz, where the detected power reaches a local maximum, standing out significantly from the surrounding noise level. This also matches with the theoretical value of the range frequency calculated using Equation (10). This peak corresponds to the resonant frequency at which the object's reflected signal is most powerfully received, and it represents the radar's ability to identify the presence of an underwater object within the specified salinity conditions. The peak's sharpness suggests a system with a narrowband response at the resonant frequency, indicative of a high-quality factor which is desirable for distinguishing the signal from the background noise. The noise floor, represented by the green curve, remains relatively constant across the frequency spectrum, with minor fluctuations that do not exhibit any systematic frequency dependence. The consistent separation between the signal and noise curves across the frequency range, particularly at the resonant peak, indicates a good signal-to-noise ratio (SNR) which is critical for reliable identification. The graph elucidates the impact of environmental conditions, such as water salinity, on the photonic radar's performance. The attenuation due to salinity is quantified by the difference in power levels between the signal peak and the noise floor. The results suggest that the system maintains functional capabilities despite the attenuation effects introduced by the underwater envi-

ronment's salinity. For testing the proposed system under varying attenuation levels, we have tested different levels of salinity, as shown in Figure 6.

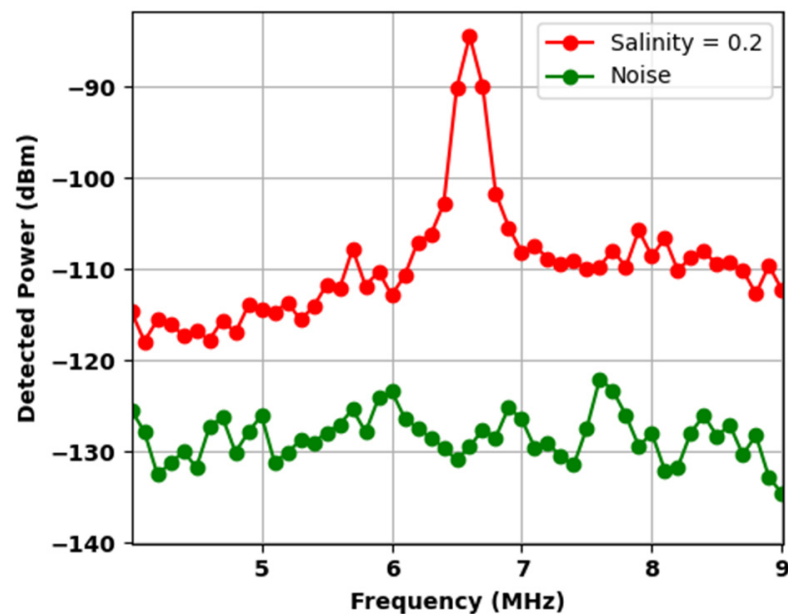


Figure 5. Target detection in clear ocean conditions.

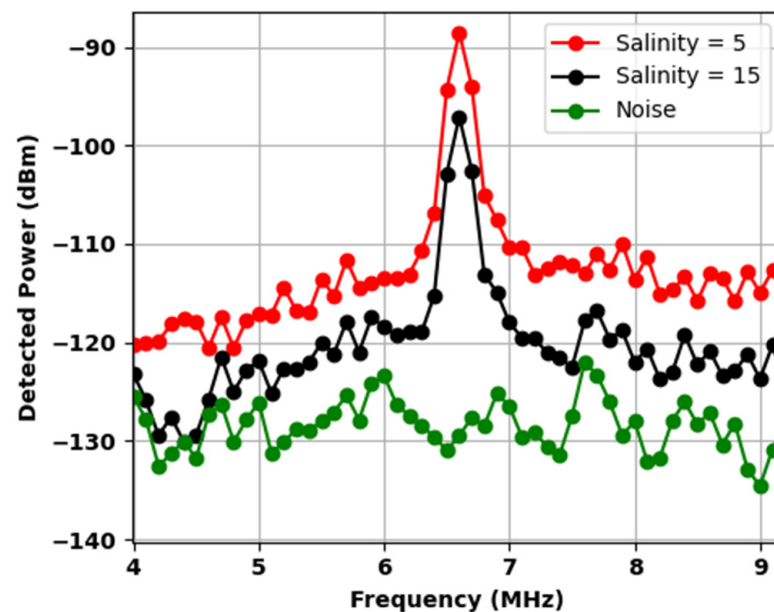


Figure 6. Target detection under varying salinity levels.

The displayed graph illustrates the capabilities of the photonic radar system under varying levels of salinity, showcasing the system's response across a frequency range of 4 to 9 MHz. The detected power, expressed in dBm, is plotted on the Y-axis, while the frequency is represented on the X-axis. Two distinct curves indicate the power at salinity levels of 5 g/L and 15 g/L, depicted by red and black markers, respectively. Additionally, the noise floor is represented by green markers. At both salinity levels, the system exhibits a pronounced peak in power at around 7 MHz, indicative of the resonant frequency. Notably, the peak corresponding to a salinity of 5 g/L (red curve) is higher than the one for 15 g/L (black curve), suggesting that increased salinity levels result in greater signal attenuation,

as expected due to the increased absorption and scattering effects in saltier waters. The peak power at 5 g/L salinity is closer to  $-95$  dBm, while at 15 g/L, the peak drops to approximately  $-105$  dBm. This 10 dB difference can be significant, implying that the radar's sensitivity and effectiveness are inversely proportional to the salinity of the water. These results underscore the importance of accounting for environmental conditions when calibrating and deploying photonic radar systems for underwater applications. The noise floor remains consistent across the frequency spectrum for both salinity levels and is distinguishable from the signal peaks, which is crucial for the radar's ability to discern between true object echoes and background noise.

The graph in Figure 7 demonstrates the relationship between signal-to-noise ratio (SNR) and target range for the photonic radar system, with measurements taken at four different salinity levels (0.2, 5, 10, and 15 g/L). The SNR is measured in decibels (dB) and plotted on the Y-axis, while the target range in meters is presented on the X-axis, spanning from 4 to 12 m. The four curves, each representing a different salinity level, show a clear trend: the SNR decreases as the range increases. This is expected due to the propagation loss that naturally occurs as the distance between the radar system and the target becomes greater. Additionally, each increase in salinity level showed a corresponding decrease in SNR, indicative of the attenuating effect of salt in the water, which absorbs and scatters the photonic signal. The curve for the lowest salinity level of 0.2 g/L (red) starts with the highest SNR, indicating that under nearly fresh water conditions, the system performs optimally. As salinity increases to 5 g/L (black), 10 g/L (blue), and 15 g/L (yellow), the SNR for a given range decreases, demonstrating the compounding effect of range and salinity on signal identification. At the shortest range of 4 m, all salinity levels maintained an SNR above 10 dB, suggesting robust capabilities close to the radar. However, as the range extended to 12 m, the SNR for the highest salinity level fell below 0 dB, indicating that the signal is no longer distinguishable from the noise. This threshold, where the SNR dips below 0 dB, is reached at progressively shorter ranges as salinity increases, with the 0.2 g/L curve maintaining an SNR above this threshold for all displayed ranges.

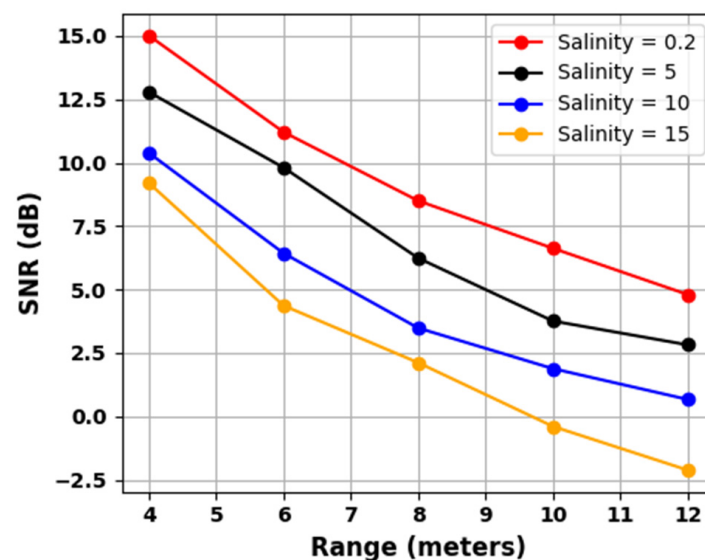


Figure 7. SNR vs. range under varying salinity levels.

The enhanced discussion links observed results with practical implications for underwater vehicle detection and navigation, focusing on the photonic radar system's applications and limitations in high-salinity waters. The system shows promise for marine exploration, environmental monitoring, and defense in low-salinity conditions, but faces challenges in extended-range operations as salinity levels increase. Environmental considerations, such as signal attenuation due to salinity, are crucial for deployment. While

the system demonstrates sensitivity and selectivity in low- to moderate-salinity waters, further development is needed for high-salinity scenarios. The findings have implications for various naval and marine applications, with the system's adaptability to environmental conditions being key for effective monitoring, navigation, and defense.

#### 4. Conclusions

In conclusion, this research has successfully demonstrated the capabilities of a novel photonic radar system for underwater vehicle detection across various salinity levels and distances. The system's performance, evaluated through experiments, provides insights into the impact of environmental factors on underwater radar detection. The analysis revealed that the system could distinguish between the signal and noise floor across the tested frequency range. At a salinity level of 5 g/L, the detected power peaked at around  $-95$  dBm, while at 15 g/L, it dropped to approximately  $-105$  dBm, indicating significant salinity impact on signal attenuation. The noise floor remained below  $-130$  dBm across all frequencies, ensuring a robust detection threshold. The SNR evaluation against target range showed a decreasing trend with increasing range and salinity. The system demonstrated strong detection capabilities within short ranges, maintaining an SNR above 10 dB for ranges up to 4 m, even at the highest tested salinity of 15 g/L. However, at longer ranges, the SNR dropped below 0 dB, highlighting challenges posed by higher salt concentrations and distances. These findings suggest that the photonic radar system is highly sensitive and selective under various saline conditions, but performance degradation at extended ranges and higher salinity levels indicate a need for improved signal processing and system optimization. The system shows promise for near-range applications in low- to moderate-salinity waters and potential for the early detection of underwater threats. For extended ranges, especially in high-salinity scenarios, further development is needed. This study lays the groundwork for future enhancements in photonic radar technology, aiming to overcome environmental attenuation effects and provide reliable, long-range detection capabilities in diverse underwater environments.

**Author Contributions:** Conceptualization, A.A.; Validation, A.A.; Data curation, H.Ş.B.; Writing—original draft, A.A.; Writing—review & editing, A.A.; Supervision, H.Ş.B. All authors have read and agreed to the published version of the manuscript.

**Funding:** This research received no external funding.

**Institutional Review Board Statement:** Not applicable.

**Informed Consent Statement:** Not applicable.

**Data Availability Statement:** The data presented in this study are available on request from the corresponding author.

**Conflicts of Interest:** The authors declare no conflict of interest.

#### References

1. Mohsan, S.A.H.; Li, Y.; Sadiq, M.; Liang, J.; Khan, M.A. Recent advances, future trends, applications and challenges of internet of underwater things (IoUT): A comprehensive review. *J. Mar. Sci. Eng.* **2023**, *11*, 124. [CrossRef]
2. Zhang, B.; Ji, D.; Liu, S.; Zhu, X.; Xu, W. Autonomous underwater vehicle navigation: A review. *Ocean Eng.* **2023**, *273*, 113861. [CrossRef]
3. Bae, I.; Hong, J. Survey on the Developments of Unmanned Marine Vehicles: Intelligence and Cooperation. *Sensors* **2023**, *23*, 4643. [CrossRef] [PubMed]
4. Yang, S.; Liu, P.; Lim, T.H. IoT-based underwater robotics for water quality monitoring in aquaculture: A survey. In Proceedings of the The 11th International Conference on Robot Intelligence Technology and Applications (RiTA 2023), Taicang, China, 31 August 2023.
5. Conde, M.S. Coordinated Control of Autonomous Underwater Vehicles. 2023. Available online: <https://repositorio-aberto.up.pt/bitstream/10216/153622/2/647459.pdf> (accessed on 15 November 2023).
6. Li, J.; Zhang, G.; Jiang, C.; Zhang, W. A survey of maritime unmanned search system: Theory, applications and future directions. *Ocean. Eng.* **2023**, *285*, 115359. [CrossRef]

7. Wibisono, A.; Piran, M.J.; Song, H.-K.; Lee, B.M. A survey on unmanned underwater vehicles: Challenges, enabling technologies, and future research directions. *Sensors* **2023**, *23*, 7321. [[CrossRef](#)] [[PubMed](#)]
8. Bobkov, V.; Kudryashov, A.; Inzartsev, A. A Technique to Navigate Autonomous Underwater Vehicles Using a Virtual Coordinate Reference Network during Inspection of Industrial Subsea Structures. *Remote. Sens.* **2022**, *14*, 5123. [[CrossRef](#)]
9. Agarwala, N. Using Robotics to Achieve Ocean Sustainability During the Exploration Phase of Deep Seabed Mining. *Mar. Technol. Soc. J.* **2023**, *57*, 130–150. [[CrossRef](#)]
10. Browne, K.; Raff, M. The Protection of Underwater Cultural Heritage—Future Challenges. In *International Law of Underwater Cultural Heritage: Understanding the Challenges*; Springer: Berlin/Heidelberg, Germany, 2023; pp. 591–665.
11. Yuan, S.; Li, Y.; Bao, F.; Xu, H.; Yang, Y.; Yan, Q.; Zhong, S.; Yin, H.; Xu, J.; Huang, Z.; et al. Marine environmental monitoring with unmanned vehicle platforms: Present applications and future prospects. *Sci. Total. Environ.* **2023**, *858*, 159741. [[CrossRef](#)]
12. Felemban, E.; Shaikh, F.K.; Qureshi, U.M.; Sheikh, A.A.; Bin Qaisar, S. underwater sensor network applications: A comprehensive survey. *Int. J. Distrib. Sens. Netw.* **2015**, *11*, 896832. [[CrossRef](#)]
13. Watson, S.; Duecker, D.A.; Groves, K. Localisation of Unmanned underwater vehicles (UUVs) in complex and confined environments: A review. *Sensors* **2020**, *20*, 6203. [[CrossRef](#)]
14. Bai, X.; Liang, Z.; Zhu, Z.; Schwing, A.; Forsyth, D.; Gruev, V. Polarization-based underwater geolocalization with deep learning. *eLight* **2023**, *3*, 15. [[CrossRef](#)]
15. Ali, M.F.; Jayakody, D.N.K.; Li, Y. Recent trends in underwater visible light communication (UVLC) systems. *IEEE Access* **2022**, *10*, 22169–22225. [[CrossRef](#)]
16. Jiang, S. On securing underwater acoustic networks: A survey. *IEEE Commun. Surv. Tutor.* **2018**, *21*, 729–752. [[CrossRef](#)]
17. Jiang, S. On reliable data transfer in underwater acoustic networks: A survey from networking perspective. *IEEE Commun. Surv. Tutor.* **2018**, *20*, 1036–1055. [[CrossRef](#)]
18. Awan, K.M.; Shah, P.A.; Iqbal, K.; Gillani, S.; Ahmad, W.; Nam, Y. Underwater wireless sensor networks: A review of recent issues and challenges. *Wirel. Commun. Mob. Comput.* **2019**, *2019*, 6470359. [[CrossRef](#)]
19. Melodia, T.; Kulhandjian, H.; Kuo, L.C.; Demirors, E. Advances in underwater acoustic networking. In *Mobile Ad Hoc Networking: Cutting Edge Directions*; Wiley: Hoboken, NJ, USA, 2013; pp. 804–852.
20. Zeng, Z.; Fu, S.; Zhang, H.; Dong, Y.; Cheng, J. A Survey of underwater optical wireless communications. *IEEE Commun. Surv. Tutor.* **2016**, *19*, 204–238. [[CrossRef](#)]
21. Al-Zhrani, S.; Bedaiwi, N.M.; El-Ramli, I.F.; Barasheed, A.Z.; Abduldaiem, A.; Al-Hadeethi, Y.; Umar, A. Underwater optical communications: A brief overview and recent developments. *Eng. Sci.* **2021**, *16*, 146–186. [[CrossRef](#)]
22. Ganesh, P.S.S.P.; Venkataraman, H. RF-based wireless communication for shallow water networks: Survey and analysis. *Wirel. Pers. Commun.* **2021**, *120*, 3415–3441. [[CrossRef](#)]
23. Murugan, K.H.S.; Sharma, A.; Malhotra, J. Performance analysis of 80 Gbps Ro-FSO system by incorporating hybrid WDM-MDM scheme. *Opt. Quantum Electron.* **2020**, *52*, 505. [[CrossRef](#)]
24. Fang, C.; Li, S.; Wang, Y.; Wang, K. High-Speed Underwater Optical Wireless Communication with Advanced Signal Processing Methods Survey. *Photonics* **2023**, *10*, 811. [[CrossRef](#)]
25. Mohsan, S.A.H.; Mazinani, A.; Sadiq, H.B.; Amjad, H. A survey of optical wireless technologies: Practical considerations, impairments, security issues and future research directions. *Opt. Quantum Electron.* **2022**, *54*, 187. [[CrossRef](#)]
26. Gkoura, L.K.; Roumelas, G.; Nistazakis, H.E.; Sandalidis, H.G.; Vavoulas, A.; Tsigopoulos, A.D.; Tombras, G.S.; Tombras, G.S. Underwater optical wireless communication systems: A Concise Review. In *Turbulence Modelling Approaches—Current State, Development Prospects, Applications*; Volkov, K., Ed.; IntechOpen: London, UK, 2007. [[CrossRef](#)]
27. Mohsan, S.A.H.; Mazinani, A.; Othman, N.Q.H.; Amjad, H. Towards the internet of underwater things: A comprehensive survey. *Earth Sci. Inform.* **2022**, *15*, 735–764. [[CrossRef](#)]
28. Zhang, Y.; Carballo, A.; Yang, H.; Takeda, K. Perception and sensing for autonomous vehicles under adverse weather conditions: A survey. *ISPRS J. Photogramm. Remote. Sens.* **2023**, *196*, 146–177. [[CrossRef](#)]
29. Sharma, A.; Malhotra, J. Performance enhancement of photonic radar sensor for detecting multiple targets by incorporating mode division multiplexing. *Opt. Quantum Electron.* **2022**, *54*, 410. [[CrossRef](#)]
30. Sharma, A.; Malhotra, J. Evaluating the effects of material reflectivity and atmospheric attenuation on photonic radar performance in free space optical channels. *J. Opt. Commun.* **2023**. [[CrossRef](#)]
31. Sharma, A.; Malhotra, J. Performance Investigation of Photonic Radar for Autonomous Vehicles' Application Under Various Degrading Conditions. In *Signals, Machines and Automation, Proceedings of the SIGMA 2022, Delhi, India, 5–6 August 2022*; Lecture Notes in Electrical Engineering; Springer: Singapore, 2023; pp. 505–512.
32. Bae, Y.; Shin, J.; Lee, S.-G.; Kim, H. Field Experiment of Photonic Radar for Low-RCS Target Detection and High-Resolution Image Acquisition. *IEEE Access* **2021**, *9*, 63559–63566. [[CrossRef](#)]
33. Sharma, A.; Chaudhary, S.; Malhotra, J.; Parnianifard, A.; Kumar, S.; Wuttisittikulij, L. Impact of Bandwidth on Range Resolution of Multiple Targets Using Photonic Radar. *IEEE Access* **2022**, *10*, 47618–47627. [[CrossRef](#)]
34. Sharma, A.; Malhotra, J. Simulative investigation of FMCW based optical photonic radar and its different configurations. *Opt. Quantum Electron.* **2022**, *54*, 233. [[CrossRef](#)]
35. Sharma, A.; Chaudhary, S.; Malhotra, J.; Parnianifard, A.; Wuttisittikulij, L. Measurement of target range and doppler shift by incorporating PDM-enabled FMCW-based photonic radar. *Optik* **2022**, *262*, 169191. [[CrossRef](#)]

36. Chaudhary, S.; Sharma, A.; Khichar, S.; Tang, X.; Wei, X.; Wuttisittikulij, L. High Resolution-Based Coherent Photonic Radar Sensor for Multiple Target Detections. *J. Sens. Actuator Netw.* **2022**, *11*, 49. [[CrossRef](#)]
37. Sharma, A.; Malhotra, J.; Khichar, S.; Parnianifard, A.; Chaudhary, S. Highly efficient frequency modulated continuous wave based photonic radar by incorporating electronic equalization scheme. *Opt. Quantum Electron.* **2023**, *55*, 797. [[CrossRef](#)]
38. Kumari, A.; Kumar, A.; Reddy, G.S.T. Performance analysis of the coherent FMCW photonic radar system under the influence of solar noise. *Front. Phys.* **2023**, *11*, 1215160. [[CrossRef](#)]
39. Bosu, R.; Prince, S. Perturbation methods to track wireless optical wave propagation in a random medium. *J. Opt. Soc. Am. A* **2016**, *33*, 244–250. [[CrossRef](#)] [[PubMed](#)]
40. Kaushal, H.; Kaddoum, G. Underwater optical wireless communication. *IEEE Access* **2016**, *4*, 1518–1547. [[CrossRef](#)]
41. Jerlov, N.G. *Marine Optics*; Elsevier: Amsterdam, The Netherlands, 1976.
42. Hulburt, E.O. Optics of distilled and natural water. *J. Opt. Soc. Am.* **1945**, *35*, 698–705. [[CrossRef](#)] [[PubMed](#)]
43. Korotkova, O.; Farwell, N.; Shchepakina, E. Light scintillation in oceanic turbulence. *Waves Random Complex Media* **2012**, *22*, 260–266. [[CrossRef](#)]
44. Jamali, M.V.; Nabavi, P.; Salehi, J.A. MIMO underwater visible light communications: Comprehensive channel study, performance analysis, and multiple-symbol detection. *IEEE Trans. Veh. Technol.* **2018**, *67*, 8223–8237. [[CrossRef](#)]
45. Borowski, B. Characterization of a very shallow water acoustic communication channel. In Proceedings of the OCEANS 2009, Biloxi, MS, USA, 26–29 October 2009.
46. Boyd, C.E. *Water Quality: An Introduction*; Springer Nature: Berlin/Heidelberg, Germany, 2019.
47. Elghandour, A.H.; Ren, C.D. Modeling and comparative study of various detection techniques for FMCW LIDAR using optisystem. In Proceedings of the International Symposium on Photoelectronic Detection and Imaging 2013: Laser Sensing and Imaging and Applications, Beijing, China, 25 June 2013; p. 890529.
48. Keiser, G. *Optical Communications Essentials*; McGraw-Hill Education: New York, NY, USA, 2003.
49. Elghandour, A.; Dianren, C. Study on detection techniques of distance and velocity by chirped LIDAR. In Proceedings of the 2012 International Conference on Optoelectronics and Microelectronics, Changchun, China, 23–25 August 2012; pp. 354–358.
50. Chaudhary, S.; Wuttisittikulij, L.; Saadi, M.; Sharma, A.; Al Otaibi, S.; Nebhen, J.; Rodriguez, D.Z.; Kumar, S.; Sharma, V.; Phanomchoeng, G.; et al. Coherent detection-based photonic radar for autonomous vehicles under diverse weather conditions. *PLoS ONE* **2021**, *16*, e0259438. [[CrossRef](#)]
51. Agrawal, G.P. *Fiber-Optic Communication Systems*; John Wiley & Sons: New York, NY, USA, 2012; Volume 222.

**Disclaimer/Publisher’s Note:** The statements, opinions and data contained in all publications are solely those of the individual author(s) and contributor(s) and not of MDPI and/or the editor(s). MDPI and/or the editor(s) disclaim responsibility for any injury to people or property resulting from any ideas, methods, instructions or products referred to in the content.